CrystEngComm

RSC Publishing

PAPER

View Article Online
View Journal | View Issue

Cite this: *CrystEngComm*, 2013, **15**, 6695

Control of growth mode and crystallinity of aluminium-doped zinc oxide thin film at room temperature by self-assembled monolayer assisted modulation on substrate surface energy†

Thieu Thi Tien Vo,[a] Yu-Hsuan Ho,[a] Pao-Hung Lin[b] and Yian Tai*[a]

Received 3rd May 2013,
Accepted 20th June 2013

DOI: 10.1039/c3ce40781k

www.rsc.org/crystengcomm

In this work, aluminium-doped zinc oxide (AZO) was deposited *via* RF magnetron sputtering on glass substrates having different surface energies at room temperature. The different surface energies were developed by passivation of alkylsilane self-assembled monolayers (SAMs) with various hydrocarbon chain lengths on substrates. The effects of substrate surface energies on growth mode and crystallinity of AZO films have been characterized. This study confirmed that a film growth mode can be gradiently controlled between intermediate Stransi–Krastanov mode and Volmer–Weber mode based on the modulation of surface energies of the substrates without varying the process temperature. In addition, the crystallinity of the corresponding AZO films can be improved with respect to the change of the substrate surface energy. Thus, the electrical properties can be improved as well. Our study led to the conclusion that AZO films can be designed to achieve a desired crystalline orientation and electrical properties without varying the growth temperature.

Introduction

Transparent conducting oxide (TCO) thin films have received extensive research interest due to their versatile applications in electronic devices and solar cells.[1–4] Comparing to tin-doped indium oxide (ITO), aluminium-doped zinc oxide (AZO) has recently gained much more attention because it is a nontoxic, low-cost, abundant material with high optical transmittance in the visible and near-infrared (IR) regions (bandgap = 3.4–3.9 eV), and has low electrical resistivity and high thermal stability.[5–11] With an interest in fundamental properties and applications, significant efforts have been made in the investigations of the growth of AZO thin films. While polycrystalline AZO may have sufficient properties for some applications and studies, the highly crystalline films are most attractive due to their superior optical and electrical properties.

AZO thin films can be prepared by various methods, such as aluminium incorporation in ZnO following different physical and chemical techniques. These include DC and RF magnetron sputtering,[12,13] pulsed laser ablation,[14] chemical vapor deposition,[15] chemical beam deposition,[16] sol–gel,[17] electroless technique,[18] and spray pyrolysis.[19] The opto-electrical properties of the AZO films are highly related to their crystallinity. AZO films with preferential (002) orientation, a well-defined *c*-axis perpendicular to the substrate surface, were identified to have low resistivity and high transmittance.[20,21] Therefore, producing high quality AZO thin films with preferential (002) orientation is of tremendous importance. To successfully improve the quality of AZO thin films, two approaches have been utilized in general; *in situ* and *ex situ* methods[22]. The *in situ* method involves substrate heating (usually) in oxygen ambience during film deposition, and the *ex situ* approach requires post-annealing after the film fabrication. However, these two approaches are not suitable for AZO film deposition on the substrates which are sensitive to heat (*e.g.* flexible substrates). From this aspect, RF magnetron sputtering is the preferred method because it offers room-temperature processing and versatile adjustment of processing parameters such as bias voltage or oxygen control.[10,23–28] However, low temperature deposition usually yields amorphous materials with high resistivity, indicating no direct control on crystal growth by this method, which severely affects the performances of AZO films.[29] Thus, a suitable method for the fabrication of high crystallinity AZO films without heating the substrate is an immense challenge.

On the other hand, in the past two decades, self-assembled monolayers (SAMs) have been studied intensively because the

[a]*Department of Chemical Engineering, National Taiwan University of Science and Technology, 43 Keelung Road Sec. 4, Taipei-106, Taiwan.*
E-mail: ytai@mail.ntust.edu.tw; Fax: +886-2-2737-6644; Tel: +886-2-2737-6620
[b]*Department of Electronic and Computer Engineering, National Taiwan University of Science and Technology, 43 Keelung Road, Taipei-106, Taiwan*

† Electronic supplementary information (ESI) available. See DOI: 10.1039/c3ce40781k

SAM technique provides a unique opportunity to manipulate the physical and chemical properties of surfaces on a variety of substrates such as wetting, adhesion, lubrication, and corrosion, which are encountered in chemical sensors, organic electronics, biomedical devices, and synthesis of nanomaterials.[29–33] The SAM technique has been applied to improve the quality of thin films at ambient conditions. Because of changes in surface properties, crystal growth on SAM functionalized surfaces can also be controlled. For example, by changing the polarity of SAMs at ambient conditions, interconversion of the crystal structure of AZO thin films can be achieved.[29]

In this work, we demonstrated that the growth mode and the crystallinity of the AZO film on glass can be improved by properly modulating the surface energy of a glass substrate. We investigated the effect of surface energy of glass substrates on AZO thin film fabrication at room temperature by RF sputtering. The variation of the surface energies was achieved by varying the chain length of alkylsilane SAMs growing on substrates. The properties of alkylsilane SAMs on glass substrate and the structural, electrical and optical properties of AZO films were characterized by contact angle (CA), X-ray photoelectron spectroscopy (XPS), X-ray diffraction (XRD), scanning electron microscope (SEM), Hall measurement and ultraviolet-visible spectroscopy (UV-Vis). The results shown that the growth mode and the crystallinity of the AZO films changes with respect to the change of the substrate surface energy. Thus, the electrical and optical properties of the AZO film can be varied.

Experimental

Materials

All glass substrates used for the deposition were purchased from Corning and were cut into 2 × 2 cm^2 pieces. *n*-Propyltriethoxysilane (C3-SAM, 97%, Aldrich), *n*-octyltriethoxysilane (C8-SAM, 97%, TCI), triethoxytetradecylsilane (C12-SAM, 95%, Alfa Aesar), and *n*-octadecyltriethoxysilane (C18-SAM, 90%, Acros Organics) were used as received. Acetone, 2-propanol and decane were purchased from Acros Organics and were either of semiconductor or reagent grade (99%).

Fabrication of SAMs

The surfaces of glass substrates were cleaned in an ultrasonic bath for 15 minutes with detergent, deionized water, acetone and 2-propanol respectively and then blown dry with nitrogen. After that, the glass substrates were immersed into solutions of SAM molecules in decane for 24 h. After removing from the solutions, all glass substrates were rinsed with decane and blown dry by constant N_2 flow.

Fabrication of AZO films

AZO thin films were deposited on pristine glass substrate and glass substrates modified by different chain length of alkylsilane SAMs at room temperature using RF sputtering. A 2 inch ceramic target of 98 : 2 wt% ZnO/Al_2O_3 (99.99%, Cathay Advanced Materials Limited) was loaded on the cathode, placed 50 mm from the substrate stage, using a plasma power of 30 W. A shutter was placed immediately above the sample to ensure the deposition started only after the equilibrium was reached. The sputter chamber was evacuated to 1.0×10^{-6} Torr by using a turbomolecular pump, and then back filled with Ar to 5.0×10^{-3} Torr. The substrates were maintained at room temperature (RT) during the entire deposition using a remote temperature controller.

Characterization

The chemical composition of samples was analyzed by X-ray photoelectron spectroscopy (XPS) (VG-Thermo Theta Probe spectrometer) with monochromatic Al Kα as an X-ray source. The surface morphology of SAMs modified glass was investigated by atomic force microscopy (AFM) (Bruker, Dimension Icon®). The electrical properties were measured using Ecopia HMS-3000 Hall measurement and four-point probe instruments. The optical measurements were performed with a JASCO V-670 UV-Vis spectrometer. The morphology, thickness and atomic composition of the films were determined using a Field Emission Scanning Electron Microscope (JEOL JSM-6500F) and the crystallinity was investigated by subjecting the samples to X-ray diffraction (XRD) (PANalytical X'Pert PRO).

The critical surface tension was obtained from the so-called Zisman plot method[34] by calculation from the results of contact angles measured by deionized (DI) water, diiodomethane (MI), 1,6-dibromohexane (HB), and hexadecane (HD).

Results and discussion

The water contact angles (CA) of the pristine and SAMs with various chain lengths modified glass substrates are shown in Fig. 1(a). The pristine glass substrate exhibited a hydrophilic surface with a low contact angle of $\sim 10^\circ$, which can be attributed to the generation of hydroxyl groups on the glass surface due to UV/ozone treatment. However, the CA increased drastically to over 90° upon the passivation of SAMs on the glass substrates. Such a result is rational since hydrocarbon species are hydrophobic. Moreover, the results showed that the water CA increased with respect to the increase of hydrocarbon chain length of SAMs. In general, the contact angle is determined by the properties of surface functional groups and not by the alkyl chain length. However, the alkyl chain affects indirectly on the surface properties through ordering, packing, and tilt of the SAM on substrates.[35] The critical surface tensions with respect to the pristine and SAMs-modified glass were deduced by the Zisman plots as demonstrated in Fig. 1(b), and their corresponding values together with the CAs are revealed in Fig. 1(c). It was found that the contact angles increased and the critical surface tensions decreased with the increase in hydrocarbon chain length of alkylsilane SAMs. Since all SAMs have no functional group other than $-CH_3$ in our study, it is assured that passivation of various SAMs on glass only varies their surface energies without changing the surface dipole moment.

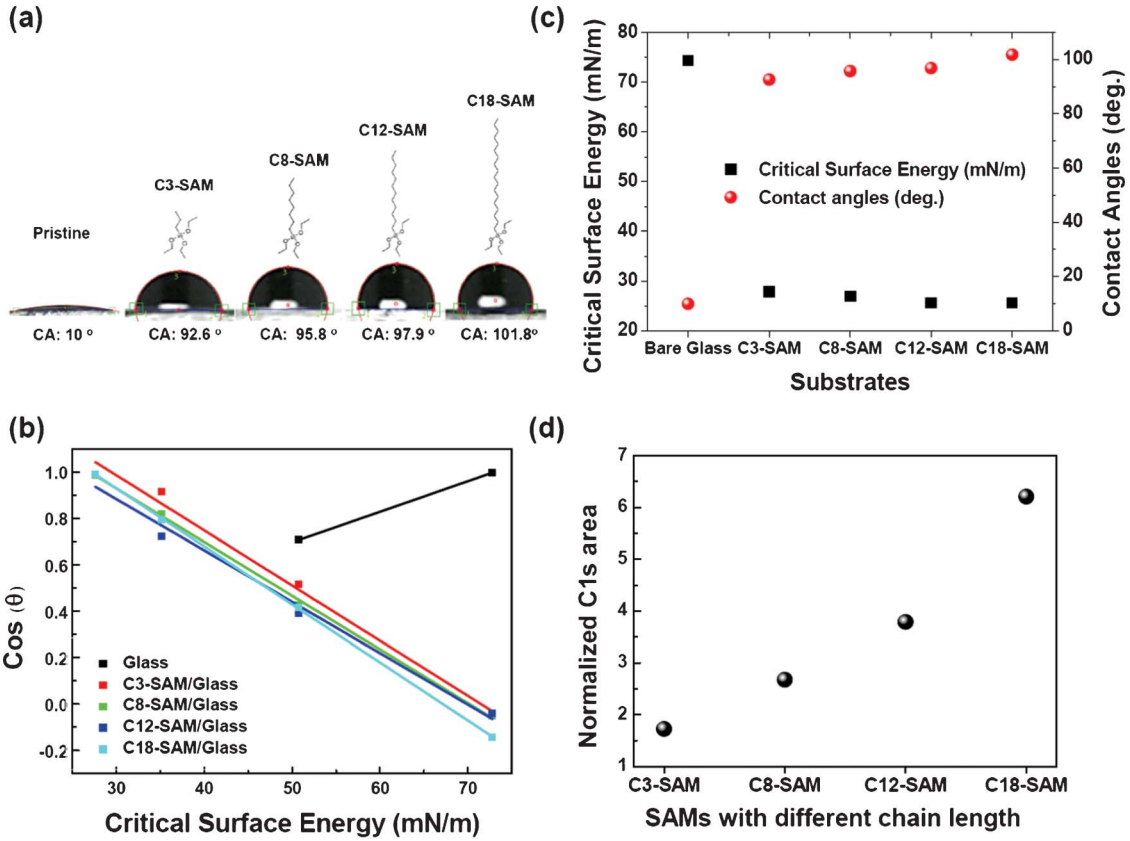

Fig. 1 The chemical structures of alkylsilane molecules, and the water contact angles of the pristine and their SAMs modified glass substrates (a), Zisman plots for calculating the critical surface energies of pristine glass, C3-SAM, C8-SAM, C12-SAM, and C18-SAM (b), the water contact angles and the critical surface energies of pristine and different SAMs modified glass substrates (c), and the normalized C 1s area ratios of various SAMs on glass substrates (d).

To investigate whether these SAMs grow well on glass or not, we performed XPS analysis. The C 1s spectra featuring SAMs with different chain lengths are demonstrated in Fig. S1 in the ESI.† The results revealed in Fig. 1(d) showed that the normalized C 1s intensity of various alkylsilane SAMs increased with the increment of carbon chain length of SAM molecules, which confirmed that the SAMs were fabricated well on glass. Moreover, the surface morphologies of the pristine and SAMs modified glass were investigated using AFM, and the results are demonstrated in Fig. S2 in the ESI.† All SAMs modified glass substrates are flatter than the pristine glass as they exhibited lower surface roughness (<2.0 nm). This result is consistent with the previous report.[36]

The XRD measurements of AZO deposited on substrates with different surface energies are exhibited in Fig. 2. The results revealed that all the obtained AZO films deposited on pristine and various alkylsilane SAMs modified glass exhibited a major peak located at 34.22°, corresponding to the (002) plane. Other peaks exhibited at 31.45°, 36.05°, 47.30°, 56.41°, 62.53° and 67.58° correspond to (100), (101), (102), (110), (103), and (112), respectively. This indicated that all the AZO films were polycrystalline with a preferential *c*-axis growth orientation perpendicular to the substrate surface. The peak position of (002) orientation, observed at 2θ = 34.22°, was lower than that of the standard ZnO crystal (2θ = 34.45°). The ionic radii of Zn^{2+} and Al^{3+} are 72 and 53 pm, respectively, when Al atoms are substituted into the Zn site in the crystal, the length of the *c*-axis is expected to be shorter. However, the Al atoms might not only substitute the Zn site in the ZnO lattice but also occupy the interstitial sites of ZnO or segregate in the non-crystalline region of the grain boundary to form Al–O bonds.[37] It is noteworthy that the normalized intensity and the full width at half maximum (FWHM) of the XRD peak at (002) became stronger and narrower with respect to the increased chain length of SAMs as shown in Table 1, indicating the crystallinity of AZO films improved with the decrease in surface energy of the substrates. The average crystallite size d_g was calculated by using Scherrer's equation.[38]

$$d_g = \frac{K\lambda}{B\cos\theta}$$

Where λ is the X-ray wavelength (1.5406 Å), B is the FWHM and θ is the Bragg diffraction angle. It was found that the average crystallite size increases with a decrease in surface energies of the substrates as shown in Table 1.

The improved crystallinity and increased grain size of AZO films upon the decrease of surface energies of the glass substrates were possibly due to two reasons; first, it is well

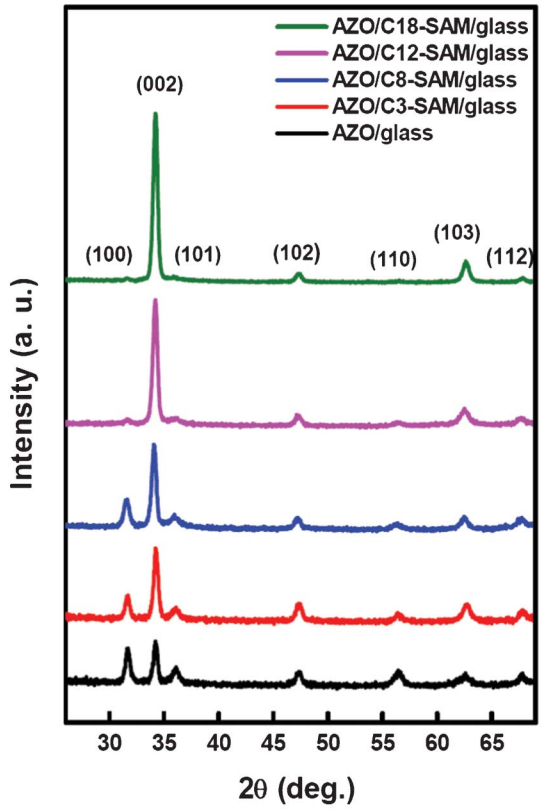

Fig. 2 XRD patterns of AZO films deposited on pristine and various SAMs modified glass substrates.

known that to achieve good crystallinity of thin film deposition on foreign substrates, a high temperature deposition or post-annealing often compensate the surface energy of the substrate, in order to increase the mobilities of deposited atoms on the substrate surface.[39] However, with the assistance of SAMs in our work, as the surface energies of glass substrates were largely reduced, the deposited species might have enough mobility even at room temperature. Second, since the SAMs are mostly hydrocarbon, the wettabilities of AZO to SAMs are poorer than that to bare glass surface. Therefore, the nucleation rate of AZO on SAMs might be reduced since it is less easy for AZO to ''stick'' on SAMs as compared to that on the pristine substrate. As a result, the Avrami theory[40,41] can be applied to interpret the increased grain size of AZO upon the decrease in surface energies herein.

Moreover, from Fig. 2 and Table 1, it is evident that the peak ratio of (100) to (002) orientations of the AZO films can be manipulated through the modulation of surface energies. With the decrease in surface energies, the peak area ratios of (100) to (002) were found to be reduced. The peak area ratio of (100)/(002) for AZO on pristine glass was 0.75, which subsequently decreased to 0.35, 0.31 and 0.04 for the film deposited on C-3, C-8, and C-12 SAM modified substrates, respectively. It is noteworthy that for the AZO film deposited on C18-SAM, the peaks (100) were found to disappear. Since the peak (100) corresponding to the crystal growth along the *a*-axis and (002) direction represent *c*-axis growth, the decrease in (100) to (002) ratio suggested a transformation of the growth direction of AZO with respect to the change of the substrate surface energies.

SEM images were collected to determine the surface morphologies and the thickness of AZO films deposited on pristine and various alkylsilane SAMs modified glass substrates. The thickness of each film was summarized in Table 1. All films are in the range of 660–720 nm and the film thickness reduced with respect to the increase in the chain length of the SAM molecules, possibly due to the different sticking coefficients of AZO to different substrates. Fig. 3(a)–(i) reveals the morphologies of AZO films deposited on bare glass, C3-SAM and C18-SAM modified glass substrates at different deposition times while the corresponding images of C8- and C12-SAMs are demonstrated in Fig. S2 in the ESI.† The surface energy of bare glass is about 74.4 mN m^{-1}, which is high enough to make the AZO film ''wet'' the substrate surface and thus exhibited a layer plus island growth mode (intermediate Stransi–Krastanov mode) in which partial two-dimensional layers are formed with some three-dimensional islands. When the glass substrates were modified by various alkylsilane SAMs, the surface energies of the substrates decreased. Therefore, the AZO did not wet the substrates. Instead, they first tend to be clustered upon the deposition to form the rod-like structure and grow in a lateral direction to increase the rod diameter. Such behavior was referred to as islands growth mode (Volmer–Weber mode). As a result, the crystal size became larger with the decrease in surface energies. Moreover, the changes in growth mode was a possible cause that led to the changes of preferential growth orientation. As a consequence, the (002) peak intensity increased with respect to the

Table 1 The parameters of AZO films deposited on pristine and various SAMs modified glass substrates obtained with XRD, XPS, and SEM

AZO thin films	Film thickness (nm)	Normalized (002) peak intensity[a]	FWHM (°)	Grain size (nm)	Peak ratio of (100)/(002)	Al in Al_2O_3/total Al[b]
AZO/glass	714	1.00	0.5	16.63	0.75	0.60
AZO/C3-SAM/glass	698	1.81	0.42	19.79	0.35	0.28
AZO/C8-SAM/glass	694	1.86	0.39	21.31	0.31	0.26
AZO/C12-SAM/glass	683	2.70	0.35	23.75	0.04	0.20
AZO/C18-SAM/glass	666	2.87	0.32	25.97	0	0.17

[a] Normalized to AZO film thickness. [b] Obtained from Al 2p XPS spectra.

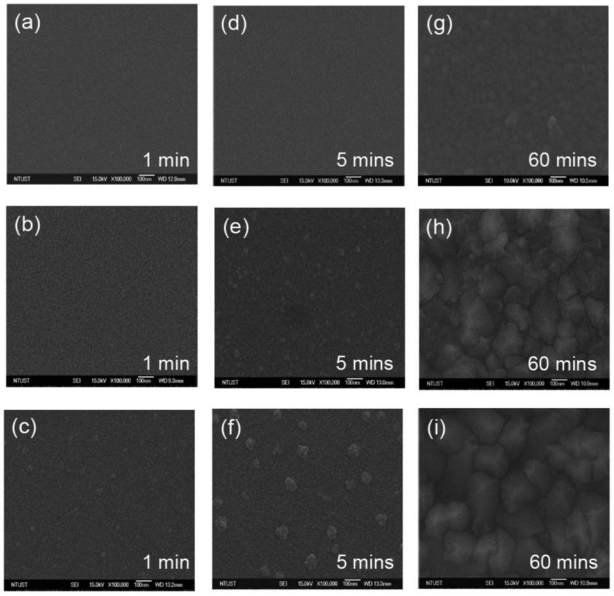

Fig. 3 SEM images of AZO films deposited at different deposition times 1, 5 and 60 minutes on pristine ((a), (d), and (g)), C3-SAM ((b), (e), and (h)), and C18-SAM ((c), (f), and (i)) modified glass substrates.

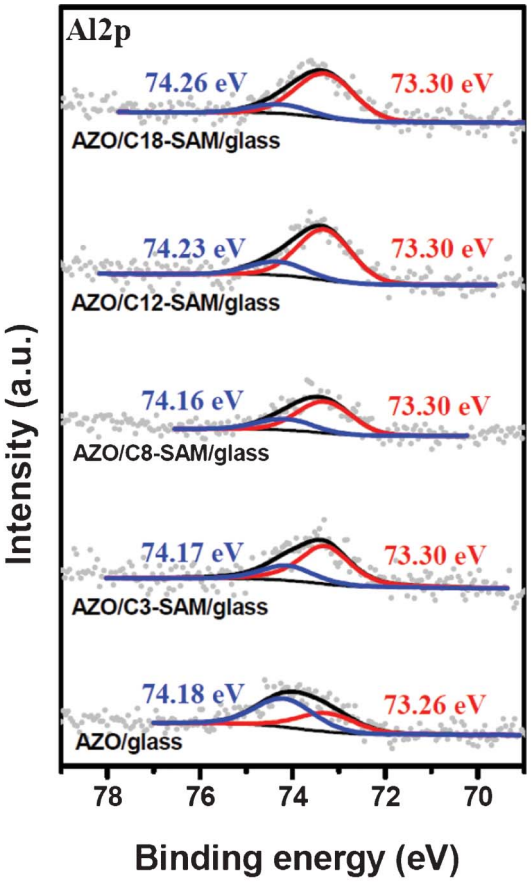

Fig. 4 Al 2p XPS spectra of AZO films deposited on various SAMs modified glass substrates.

decrease in surface energies, which confirmed the XRD results in Table 1.

It is noteworthy that at the initial stage (1 min) the pristine substrate exhibited no crystal structure of AZO on the surface as shown in Fig. 3(a). In sharp contrast, small grains can already been observed on C18-SAM modified glass at 1 min deposition time (Fig. 3(c)). Moreover, the crystal growth rate increases with respect to the decrease of surface energy as can be observed evidently in Fig. 3.

In order to examine whether Al^{3+} in Al_2O_3 was substituted into the ZnO lattice or segregated at the boundary, the chemical states of the AZO at the initial stage (AZO films deposition time = 30 s) were investigated with XPS and the results are shown in Fig. 4. The XPS spectra of the Al 2p core level were deconvoluted into two components, which were located at ~73.3 eV and ~74.2 eV, corresponding to Al–O in AZO with an oxygen-deficiency in the ZnO matrix[42] and Al_2O_3 segregated at the grain boundaries, respectively. No peak of metallic Al was observed at binding energy of ~72.7 eV.[43] The ratio of Al in Al_2O_3 (~74.2 eV) to total Al were found to be decreased with respect to the increment of hydrocarbon chain lengths of alkylsilane SAMs (Table 1), indicating that the amount of Al^{3+} ion segregated at the grain boundaries of AZO was less with the decrease in substrate surface energies; possibly due to the reason that the grain size of AZO increased with respect to the decrease in substrate energy. Therefore, the total areas of grain boundary decreased, and thus, decreased the possibility for Al^{3+} to segregate at grain boundaries.

The Hall measurements were performed with the utilization of the van der Pauw method to investigate the electrical properties of AZO films deposited on pristine and various SAMs modified surfaces. The results are summarized in Table 2. It is clear that the resistivity of AZO films decreased with the reduction of the surface energies of glass substrates due to the increased carrier mobility. Decrease in substrate surface energy resulted in better crystallinity, increased grain size and less Al^{3+} segregation of the AZO film, which allowed a decrease in carrier scattering in the film area that to be crossed by the electrons. Therefore, it led to an increase in Hall mobility and film conductivity.[44] Moreover, the reduction of surface energies could contribute to the increasing amount of Al^{3+} substituted to Zn^{2+} in the ZnO lattice as revealed in Fig. 4, which might reduce the defects in the ZnO lattice that resulted in the improvement of Hall mobility as well.

For optical properties, we performed UV-Vis transmittance measurements, and the results are revealed in Fig. 5. It is cleared that the average transmittance over the 400–800 nm range exceeds 85% for all AZO films deposited on SAMs modified glass substrate regardless of the surface energies, which meets the requirement for a transparent conducting oxide to be applied practically in a device. The transmittance of AZO films deposited on SAMs modified glass substrate was slightly improved, compared to AZO film deposited on pristine substrate, possibly due to the improved crystallinity of AZO films on SAMs modified glass.

Table 2 The electrical parameters of AZO films deposited on pristine and various SAMs modified glass substrates

AZO thin films	Carrier concentration ($\times 10^{20}$ cm^{-3})	Mobility (cm^2 V^{-1} s^{-1})	Resistivity (10^{-3} Ω cm)	Sheet resistance (Ω)
AZO/glass	2.28	2.72	10.08	141.2
AZO/C3-SAM/glass	2.31	3.24	8.35	120.3
AZO/C8-SAM/glass	2.18	3.48	8.24	118.3
AZO/C12-SAM/glass	2.46	3.76	6.76	99.0
AZO/C18-SAM/glass	2.27	4.19	6.57	98.6

The bandgap of each AZO film can be deduced from UV-Vis spectra as shown in the inset in Fig. 5. All films revealed bandgap values between 3.3 and 3.4 eV (Table S1 in ESI†), which is rational for AZO films. A trend can be observed that the bandgap decreased slightly upon the decrease of the chain length of the SAMs. It is possible due to the reason that the crystallinity diminished with the decrease of alkyl chain length, leading to the increased defect of the AZO film. Thus, the Fermi level of the AZO is altered, resulting in the reduction of bandgap.

Summary

In summary, we demonstrated the utilization of SAMs with different hydrocarbon chain lengths on glass substrates, to modulate the surface energies and the effect on AZO films deposited on those substrates thereafter. With decrease in surface energies, not only the crystallinity and the grain sizes of AZO films improved, but also the amount of Al^{3+} ion, substituted into Zn^{2+} ion sites in the ZnO lattice were increased, resulting in amplification of Hall mobility and decrease in resistivity of AZO films. Furthermore, the surface energy manipulated the growth mode and the orientations of the AZO film. Our study paves a way for the manipulation of oxide thin film structures and properties at room temperature without heating, which is crucial for the applications in flexible optoelectronics where the substrates are sensitive to heat.

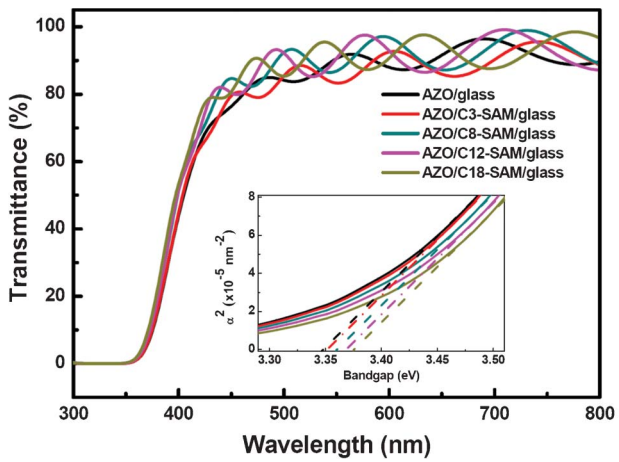

Fig. 5 The transmittance of AZO thin films deposited on pristine and various SAMs modified glass substrates.

Acknowledgements

The authors are grateful to Prof. Thomas C.-K. Yang of NTUT for the support of XRD instrumentation. This work was financially supported by the National Science Council.

References

1 H. Kim, C. M. Gilmore, J. S. Horwitz, A. Pique, H. Murata, G. P. Kushto, R. Schlaf, Z. H. Kafafi and D. B. Chrisey, *Appl. Phys. Lett.*, 2000, **76**, 259–261.
2 S. H. Jeong and J. H. Boo, *Thin Solid Films*, 2004, **447–448**, 105–110.
3 L. Kerkache, A. Layadi and A. Mosser, *J. Alloys Compd.*, 2009, **485**, 46–50.
4 S. H. Paeng, M. W. Park and Y. M. Sung, *Surf. Coat. Technol.*, 2010, **205**, S210–S215.
5 J. G. Lu, Z. Z. Ye, Y. J. Zeng, L. P. Zhu, L. Wang, J. Yuan, B. H. Zhao and Q. L. Liang, *J. Appl. Phys.*, 2006, **100**, 073714–11.
6 M. Chen, Z. L. Pei, C. Sun, L. S. Wen and X. Wang, *Mater. Lett.*, 2001, **48**, 194–198.
7 M. Purica, E. Budianu, E. Rusu, M. Danila and R. Gavrila, *Thin Solid Films*, 2002, **403–404**, 485–488.
8 V. Khranovskyy, J. Eriksson, A. Lloyd-Spetz, R. Yakimova and L. Hultman, *Thin Solid Films*, 2009, **517**, 2073–2078.
9 S. Y. Myong and K. S. Lim, *Appl. Phys. Lett.*, 2003, **82**, 3026–3028.
10 R. Wen, L. Wang, X. Wang, G. H. Yue, Y. Chen and D. L. Peng, *J. Alloys Compd.*, 2010, **508**, 370–374.
11 D.-K. Kim and H.-B. Kim, *J. Alloys Compd.*, 2012, **522**, 69–73.
12 M. Suchea, S. Christoulakis, N. Katsarakis, T. Kitsopoulos and G. Kiriakidis, *Thin Solid Films*, 2007, **515**, 6562–6566.
13 Y. E. Lee, Y. J. Kim and H. J. Kim, *J. Mater. Res.*, 1998, **13**, 1260–1265.
14 V. Srikant, V. Sergo and D. R. Clarke, *J. Am. Ceram. Soc.*, 1995, **78**, 1935–1939.
15 W.-H. Kim, W. J. Maeng, M.-K. Kim and H. Kim, *J. Electrochem. Soc.*, 2011, **158**, D495–D499.
16 H. Sato, T. Minami, S. Takata, T. Miyata and M. Ishii, *Thin Solid Films*, 1993, **236**, 14–19.

17 M. Ohyama, H. Kozuka and T. Yoko, *J. Am. Ceram. Soc.*, 1998, **81**, 1622–1632.
18 D. Ravindra and J. K. Sharma, *J. Appl. Phys.*, 1985, **58**, 838–844.
19 A. F. Aktaruzzaman, G. L. Sharma and L. K. Malhotra, *Thin Solid Films*, 1991, **198**, 67–74.
20 H. M. Zhou, D. Q. Yi, Z. M. Yu, L. R. Xiao and J. Li, *Thin Solid Films*, 2007, **515**, 6909–6914.
21 J.-M. Kim, P. Thiyagarajan and S.-W. Rhee, *Thin Solid Films*, 2010, **518**, 5860–5865.
22 D. P. Norton, *Mater. Sci. Eng., R*, 2004, **43**, 139–247.
23 J. H. Lee and J. T. Song, *Thin Solid Films*, 2008, **516**, 1377–1381.
24 M. Chen, Z. L. Pei, X. Wang, C. Sun and L. S. Wen, *Mater. Lett.*, 2001, **48**, 137–143.
25 S.-Y. Kuo, K.-C. Liu, F.-I. Lai, J.-F. Yang, W.-C. Chen, M.-Y. Hsieh, H.-I. Lin and W.-T. Lin, *Microelectron. Reliab.*, 2010, **50**, 730–733.
26 X. B. Zhang, Z. L. Pei, J. Gong and C. Sun, *J. Appl. Phys.*, 2007, **101**, 014910–7.
27 J. W. Seong, K. H. Kim, Y. W. Beag, S. K. Koh and K. H. Yoon, *J. Vac. Sci. Technol., A*, 2004, **22**, 1139–1145.
28 D. K. Kim and H. B. Kim, *J. Alloys Compd.*, 2011, **509**, 421–425.
29 Y. Tai, J. Sharma, H.-C. Chang, T. V. T. Tien and Y.-S. Chiou, *Chem. Commun.*, 2011, **47**, 1785–1787.
30 N. Rozlosnik, M. C. Gerstenberg and N. B. Larsen, *Langmuir*, 2003, **19**, 1182–1188.
31 A. Ulman, *Chem. Rev.*, 1996, **96**, 1533–1554.
32 N. Ballav, A. Terfort and M. Zharnikov, *J. Phys. Chem. C*, 2009, **113**, 3697–3706.
33 A. Singh, I. S. Lee, K. Kim and A. S. Myerson, *CrystEngComm*, 2011, **13**, 24–32.
34 W. A. Zisman, Relation of the equilibrium contact angle to liquid and solid constitution, in *Contact Angle, Wettability, and Adhesion*, American Chemical Society, Washington, DC, 1964, vol. 43, pp. 1–51.
35 D. K. Aswal, S. Lenfant, D. Guerin, J. V. Yakhmi and D. Vuillaume, *Anal. Chim. Acta*, 2006, **568**, 84–108.
36 Y. Wang and M. Lieberman, *Langmuir*, 2003, **19**, 1159–1167.
37 K. C. Park, D. Y. Ma and K. H. Kim, *Thin Solid Films*, 1997, **305**, 201–209.
38 B. D. Cullity, *Elements of X-ray Diffraction*, Addison-Wesley, 2nd, 1978, p. 102.
39 J. A. Venables, G. D. T. Spiller and M. Hanbucken, *Rep. Prog. Phys.*, 1984, **47**, 399–459.
40 M. Avrami, *J. Chem. Phys.*, 1939, **7**, 1103.
41 M. Avrami, *J. Chem. Phys.*, 1940, **8**, 212.
42 M. Chen, X. Wang, Y. H. Yu, Z. L. Pei, X. D. Bai, C. Sun, R. F. Huang and L. S. Wen, *Appl. Surf. Sci.*, 2000, **158**, 134–140.
43 C. D. Wagner, L. E. Davis, J. F. Moulder and G. E. Muilenberg, *Handbook of X-ray Photoelectron Spectroscopy*, PerkinElmer Corporation, Eden Prairie, Mn, 1979, pp. 50–51.
44 Y. Yang, X. Zeng, Y. Zeng, L. Liu and Q. Chen, *Appl. Surf. Sci.*, 2010, **257**, 232–238.